



Inhibition of Coliforms and *Escherichia coli* Bacterial Strains in Water by 3D Printed CS/GO/AgNP Filtration Membranes

Anthony C. Ogazi¹ · Peter O. Osifo¹

Accepted: 24 April 2023 / Published online: 12 May 2023
© The Author(s) 2023, corrected publication 2023

Abstract

The effect of 3D printed modified Chitosan membranes on bacterial strains by water filtration system was explored in this study. Specifically, it focused on the characterisation of 3D printed Chitosan–graphene oxide–silver nanoparticles (CS–GO–AgNP) composite membranes and the effects of Dimethylacetamide (DMAc) used as co-solvent on the performance of the CS–GO–AgNP nanocomposites. It also examined the impact of GO–AgNP on the CS matrix for inhibition of Fecal Coliforms, Total Coliforms and *Escherichia coli* (*E. coli*) bacterial strains in contaminated surface water. The increase in DMAc concentration and subsequent reduction in CS mole fraction within the ink formulation resulted to wider distribution of AgNP across membrane surface, improvement in mechanical strength and surface hydrophilicity of the modified CS membranes. Similarly, increase in GO–AgNP concentration effectively reduced the spread of the identified microorganisms. Sample B-12 with 79% CS, 21% DMAc and 1.2 ml of GO–AgNP exhibited the highest inhibition of the bacterial strains, with more than 95% of Fecal and Total Coliforms suppressed or inactivated, while 99.9% of the *E. coli* bacterial cells were completely prevented, indicating that our 3D printed modified CS membranes can effectively be used for water treatment.

Keywords 3D printing · Modified-Chitosan · DMAc · GO–AgNP · *E. coli* · Filtration membranes

Introduction

Access to potable water is essential for human health. Utilizing high-quality drinking water may provide substantial health advantages. However, microbial pollution and proliferation on surface water have long been a hazard to human health and a major social problem. The major source of fecal bacteria, including pathogens, in surface water is waste discharge from human and animal excrements which have resulted to various water borne diseases because of presence of microorganisms. Bacteria found in drinking water originate in the digestive tracts of warm-blooded animals. Sources include animals, pets and pollution owing to incorrectly constructed, failed, or overcrowded waste treatment facilities, such as private septic systems and sanitation

pipelines. According to the World Health Organization (WHO, 2003), frequent monitoring of fecal pollution in surface water is essential for protecting public health [1]. Fecal indicator bacteria (FIB), such as Total Coliforms, Fecal Coliforms, and *E. coli*, has been used for a very long time to assess Fecal pollution in surface water. Typically, FIB detection and measurement are accomplished by utilizing culture-based techniques [2]. *E. coli* identifies Fecal contamination more precisely than Total Coliforms and Fecal Coliforms and it is regularly utilize for microbial analysis.

Presently, acid/alkaline based chemical detergents and disinfectants are the most prevalent techniques for deactivating bacterial strains in industrial settings. However, their efficacy is highly dependent on temperature, pH, concentration, and exposure period of the chemicals, which are often ineffectual, remove just surface growth and make water bodies dangerous for human consumption if treated chemicals are discharged as poisonous residues. Numerous microorganisms may cling to surfaces and establish a network of bacterial cells protected by Extracellular Polymeric Substances (EPS) [3]. Polysaccharides in EPS retain water and prevent microorganisms from drying, thereby increasing the likelihood of microorganisms communicating with

✉ Anthony C. Ogazi
ogazijnr@gmail.com

✉ Peter O. Osifo
petero@vut.ac.za

¹ Department of Chemical Engineering, Vaal University of Technology, P/Bag X021, Vanderbijlpark 1900, South Africa

other bacteria and forming a complex outer matrix [4]. The complex structure of EPS matrix renders the biological fouling suppression technique ineffective. Although physical removal is the most common method for combating the EPS layer's defense strategy, the major problem is that bacteria can redeposit on any other surface and resume biofilm formation. Also, separately operating and maintaining equipment systems for biofilm control is costly [5]. Therefore, it has become imperative to develop a novel and effective method for preventing microorganisms on treatment surfaces. Recent advancements in membrane technology have shown the inclusion of nanoparticles to regulate microbial activity and decrease the threat to human health.

Chitosan (CS) a biocompatible agent and the most abundant biopolymer with a strong antibacterial activity and an extraordinary non-toxic effect, has been utilized in numerous industries, including the food, textile, biomedicine, wastewater treatment and cosmetics industries [6, 7]. However, due of its low strength and structural instability, CS has limited industrial applicability as a membrane material. To circumvent this constraint, Chitosan is often modified to increase its physicochemical characteristics. Graphene oxide (GO) is one of the compounds often used to strengthen Chitosan (CS). GO has superior mechanical strength, a wide surface area, a high adsorption capacity and antibacterial activity, which enhances the mechanical strength, stability and antibacterial characteristics of CS for its use as a material for industrial polymer membranes [8, 9].

In addition, CS is rich in hydroxyl and amino groups, which bind strongly to the oxygen of GO and increase the physical and mechanical strength of the composite film. Multiple applications, including water treatment for bacterial control, have shown antimicrobial capabilities of metallic silver or its compounds. It has been shown that the antibacterial activity of CS–AgNP–GO composites is greater than that of most antibacterial agents based only on Ag or Ag–GO [10]. Ag may interact with hydroxyl, epoxide, carbonyl and carboxyl functionalities of GO through physisorption and electrostatic binding interactions [11], as well as –OH, C–O, and –NH₂ functionalities in Chitosan [12]. According to Song et al., [13], it is known that silver nanoparticles increase surface area, which is essential for preventing bacterial growth. The findings indicated that GO–Ag nanocomposites have increased antibacterial capabilities. Khawaja et al., [14] created Chitosan–GO–AgNP composite membranes to limit pathogenic bacterial activity. Also, Goda et al. [15], fabricated silver nanoparticle-decorated N-methylene phosphonic acid chitosan/graphene films as eco-friendly antibacterial agents. The nanocomposite of Chitosan–graphene oxide doped with silver hydride has been reported to combat biological fouling [16].

There exist different traditional polymer membranes fabrication processes, which include phase inversion, track

etching, electrospinning, stretching, surface coatings of a support, and sintering. Among these, phase inversion remains the most popular approach for industrial membrane preparation in which different types of polymers may be employed for various purposes because of its simplicity and convenience. This approach involves dissolution of polymer in a solvent to create a more or less viscous solution. The mixture is then applied to a glass plate and allowed to solidify [17]. While traditional approaches provide effective membranes, it is difficult to precisely regulate the preparation conditions. Also membranes prepared by these techniques often have fragile structures with poor selective surface and sub-layers, necessitating modification. Additive manufacturing, commonly known as three-dimensional (3D) printing, is a viable alternative to phase inversion and other conventional techniques of membrane production, particularly where design complexity and intricacy are needed. Several researchers have started adopting additive manufacturing (AM) of membranes to solve these difficulties [18–20]. As a result, 3D-printed membranes have generated a lot of attention and have been the subject of several research and development investigations.

There are several methods for 3D printing, including stereolithography, digital light processing, fused deposition modeling, selective laser sintering, and multijet printing [21]. All the AM methods utilize the same fundamental principle to fabricate the final object. The entire procedure begins with a computer-aided design (CAD) model that is then converted to the stereolithography format. The obtained 3D file is then preprocessed by specialized software that defines process parameters such as 3D part orientation within the build volume and slicing parameters. The data is then sent to the 3D printer, which prints the object layer by layer [22].

Since the structure of a membrane determines its qualities, thus the requirement for careful control throughout preparation becomes very vital. Conventional membranes often have morphologies with smooth surfaces but are often characterized by uneven pore structures, including porosity, interconnectedness, dispersion, and size distribution. It is difficult to manage the preparation conditions, which results in an irregular pore structure in traditional membranes. While the stretching approach allows for the control of pore size, this pore generation process is only applicable to polymer membranes with high crystalline structures [23]. The production of 3DP membranes, on the other hand, comes from a CAD object that guarantees adequate control over all factors to generate the necessary structure. It is simple to produce 3DP membranes with embossed or grooved features, which have bigger surfaces than the conventional membranes. Researchers are particularly interested in patterned membranes because they may demonstrate enhanced transport performance, decreased

concentration polarization, and reduced fouling [24, 25]. In comparison to traditional techniques, 3D printing gives more production flexibility and makes it simpler to fabricate complicated objects.

The 3D printing of modified Chitosan membranes for oil and water separation, micropollutants degradation, dye removal and heavy metal removal [26] is gaining increasing interest. For example, Bergamonti et al. [27] printed chitosan scaffolds for antimicrobial pollutant breakdown in wastewater treatment. Sponge bionic filters were also 3D printed utilizing the chemical combination of polylactic acid-graphene oxide and Chitosan to efficiently absorb crystal violet dye in water [28]. These researchers demonstrated an efficient separation of dye from water samples. However, inactivating bacterial strains in a water filter system using 3D-printed Chitosan matrix has not been studied. In this investigation, ultraviolet (UV) inkjet 3D printing is used to fabricate modified Chitosan to restrain bacterial activities in contaminated surface water. UV inkjet technology is a well-established technique for curing printed inks and coatings in both flexography and lithography. It is the most efficient and quickest technique for converting a solvent-free monomer into a cross-linked polymer at room temperature [29]. This method initiates photochemical and chemical processes in organic materials to produce a new polymeric substance [30]. A formulation of UV-curable ink comprises a reactive monomer, a reactive oligomer, a photoinitiator, colorants and additives like surfactants and oxygen inhibitors. The foundation of a UV inkjet formulation consists of reactive monomers and oligomers, which must be functional to allow for free radical additions. Free radical and cationic curing processes are the two UV curing methods accessible. The functioning of UV-curable inkjet inks relies heavily on the effective integration of UV curing chemistry with inkjet printing technology. Viscosity, surface tension, particle size, oxygen inhibition and curing rate are formulation parameters that must be taken into account to efficiently develop UV-curable inkjet inks [31].

Dimethylacetamide (DMAc), a polar aprotic solvent, is often utilized in the manufacture of various polymers to enhance their permeability and mechanical characteristics [32, 33]. Multiple studies have shown the benefits of DMAc on polymer membranes. For instance, the effects of DMF and DMAc solvents on the electrical and thermal characteristics of PVDF–CNF composites have been investigated [34]. According to the findings, DMAc demonstrated more dispersion of the polymer composite matrix than DMF. Previous study also showed that DMAc enhanced the mechanical strength, porosity, and surface hydrophilicity of PVDF-based nanocomposite membranes treated with ZIF-8 nanocrystals [35]. In addition, the effects of increasing the DMAc/LiCl concentration in cellulose dissolving have been studied. The addition of the solvent enhanced cellulose

breakdown and enhanced diffusion via the cellulose molecular network [36].

In this study we present the use of 3D inkjet printing technological approach to produce CS/AgNP/GO composite membranes for inhibition of Fecal Coliforms, Total Coliforms and *E. coli* bacterial strains in contaminated surface water through filtration process. The modified Chitosan nanocomposites were blended with AgNP–GO and DMAc to improve the antibacterial properties and mechanical strength respectively. The fluid properties of the CS–GO–AgNP composites including surface tension, viscosity, particle size analysis, printability and drop formation for inkjet 3D printing of the nanocomposite membranes have been established in our previous study [37] (Fig. 1).

Materials and Methods

Materials

Medium molecular weight Chitosan (198KDa) with more 75% degree of deacetylation was procured from Shandong, China. Dimethylacetamide (DMAc) was purchased from Merck, South Africa. We ordered 99% sodium nitrate (NaNO_3), 99% silver nitrate (AgNO_3), and 99% potassium permanganate (KMnO_4) from Sigma-Aldrich, South Africa. Germany's Alfa Aesar provided graphite powder, 325 mesh, 99.99% pure. Glassworld South Africa provided distilled water (H_2O), hydrogen peroxide (H_2O_2), 98% sulfuric acid (H_2SO_4), glacial acetic acid and isopropyl alcohol ($\text{C}_3\text{H}_8\text{O}$). South Africa's Lab-Chem provided trisodium citrate ($\text{C}_6\text{H}_5\text{O}_3\text{Na}_3$). All of the chemicals employed were of analytical grade and were not further purified.

Preparation of GO Suspension

Graphene oxide (GO) was produced from graphite powder by modifying the Hummer and Offeman technique [38]. 1 g of graphite powder, 0.5 g of NaNO_3 and 23 ml of concentrated H_2SO_4 were introduced to a 1 L beaker flask. In a bath of freezing water, 3 g of KMnO_4 was added gradually while stirring. The reaction was maintained at a steady temperature of 35 °C with stirring for 30 min before being diluted with 46 ml of warm distillate water. Subsequently, the reaction temperature was increased to 98 °C for an additional 30 min with stirring, after which the reaction mixture was diluted with 140 ml DI water and the residual permanganate and manganese dioxide were reduced by adding 2.5 ml H_2O_2 , evidenced by a colour change from brown to yellow of the suspension. The resultant solution was centrifuged to extract solid debris, which was then washed sequentially with 100% ethanol and DI water until the pH of the supernatant reached 7. After drying the

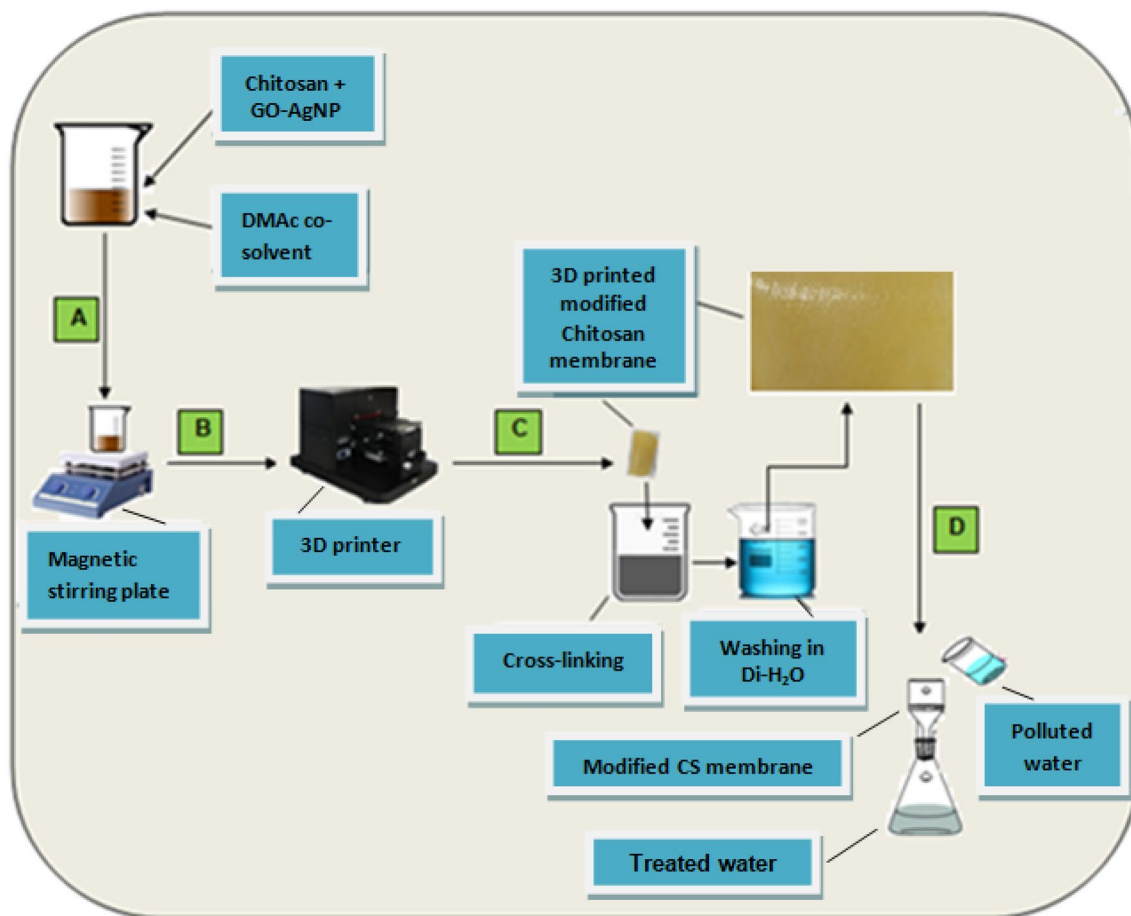


Fig. 1 Graphical abstract indicating sequence of activities

product in a vacuum oven, powdered graphite oxide was produced. A uniform GO solution with a reddish-brown colour was obtained after 90 min of ultrasonic exfoliation of graphite oxide distributed in DI water.

Synthesis of GO–AgNP

AgNP–GO nanocomposites were prepared by direct reduction of silver nitrate (AgNO_3) with trisodium citrate ($\text{C}_6\text{H}_8\text{O}_7\text{Na}$) in the presence of GO solution using a modified version of Tollens' technique [39]. Briefly, 0.4 g AgNO_3 was added to a suspension of GO containing 0.5 g GO and the mixture was vigorously combined. To achieve full reduction, 50 ml of a 0.5 mol per liter $\text{C}_6\text{H}_5\text{O}_7\text{Na}_3$ aqueous solution was added drop by drop over the course of one hour while stirring at room temperature. The mixture was centrifuged and rinsed with absolute of ethanol and DI water after 24 h of aging. It was later dried in vacuum oven to obtain GO–AgNP.

Preparation of Modified Chitosan Ink Formulation

At room temperature, 1 g of CS was dissolved in 1% acetic acid (HAc) aqueous solution and agitated consistently for 60 min. 0.5 ml of 2% (w/v) NaOH was added to the mixture to neutralize the HAc. To guarantee that air bubbles were degassed, the reaction was agitated further and left for 24 h. After stirring for one hour, 0.5 ml of a 10 w/w% AgNP–GO aqueous solution was added to 80 ml of CS solution. Before being agitated for one hour at room temperature, the resultant solution reacted with 120 ml of a 0.5% isopropyl alcohol aqueous solution. In order to avoid damage to inkjet 3D print-head, the pH of the solution was corrected to 7 using buffer solution.

3D Printing of CS–GO–AgNP Composite Films

The modified CS samples were printed using an A1630 UV type flatbed inkjet printer (Colorsun China) with an Epson L805 drop-on-demand piezoelectric inkjet print head, two

UV LED lights and AcroRIP White ver9.0 print software. Samples of modified CS inks were developed to cure when exposed to UV light with a 395 nm wavelength. The printing settings were set to 8 passes at 0.84 m per second. The print-head was elevated to 0.6 mm above the top of the material, and the jetting frequency was adjusted at 10.28 kHz. The size of the printing ink drop was 1.5 μl . With both UV lights, the ink was cured. The CS nanocomposite membranes were printed using four layers of the modified CS ink solution, with the printing procedure repeated for each layer sample. In order to ensure adequate drop formation of circular membrane diameter of 70 mm and thickness of 10 μm , the drop spacing was set to 8 μm , which ensured sufficient drop overlap and prevented composite fluids samples from evaporating before UV irradiation.

In order to ensure adequate drop formation of circular shaped membranes with diameter of approximately 70 mm and a thickness of 10 μm , the drop spacing was fixed at 8 μm to avoid ink evaporation prior to UV irradiation. The printed CS–GO–AgNP membranes were kept for 24 h at room temperature after irradiation to achieve appropriate chemical bonding. The samples were further submerged into a solution containing 0.5% wt. H_2SO_4 , 49.5% wt. acetone and 50% wt. H_2O for 30 min to ensure effective cross-linking and removal of any ungrafted composite particles and finally washed with Milli-Q water until the pH reached about 7. Figure 2 shows the inner and outer views of 3D printed images of the modified Chitosan composites with distinctive features. These samples were characterised and used for filtration analysis.

Chemical Interaction in Modified CS Composites

The possible interactions between atoms within the modified CS composite are shown in Fig. 3. The chemical structure of GO–AgNP demonstrates the interlocking of

Ag nanoparticles inside the hexagonal structure of epoxy chains to guarantee nanoparticles' stability (Fig. 3a). Since GO comprised several negatively charged molecules such as oxygen functional groups, hydroxyl, carbonyl and carboxylic acid, these groups may serve as active sites for metal cations. In the modified Chitosan solution, the surface of GO may have absorbed Ag^+ , forming Ag-GO precursors. Randomly dispersed β -linked-D-glucosamine and N-acetyl-D-glucosamine units in the CS structure may have formed covalent bonds with Dimethylacetamide (DMAc) to improve the mechanical characteristics of CS in composites [40].

DMAc is a dipolar aprotic solvent containing carbonyl and nitrogen carbon. It serves as a co-solvent and plasticizer for the matrix of CS polymer ink, among other uses. Plasticizers increase the flow and thermoplasticity of a polymer by decreasing the viscosity of the polymer melt, the glass transition temperature, the melting temperature and the elastic modulus of the final product without altering the fundamental chemical properties of the plasticized substance [41, 42]. As depicted in Fig. 3, the chemical interaction between CS and DMAc is principally driven by the presence of highly electronegative oxygen atoms in the CS structure, which might permit the production of additional carbonyl group ($\text{C}=\text{O}$). This process may remove the electron pair from the double bond to generate a partial single bond. The nitrogen atom of DMAc and the oxygen atom of the CS chain may exert a strong electrostatic attraction that attracts an electron to the nitrogen atom that forms a hydrogen bond with the hydroxyl group of CS. The methyl groups of DMAc may also engage in hydrogen bonding due to the attraction of hydrogen atoms toward electronegative oxygen and the hydroxyl atom of the CS chain. Figure 3c depicts potential chemical interactions between elements of modified CS. The reaction of hydrogen-amide ($\text{H}-\text{N}$) and hydrogen–oxygen interaction ($\text{O}-\text{H}$) may have resulted in the formation of

Fig. 2 3D printed modified Chitosan membranes

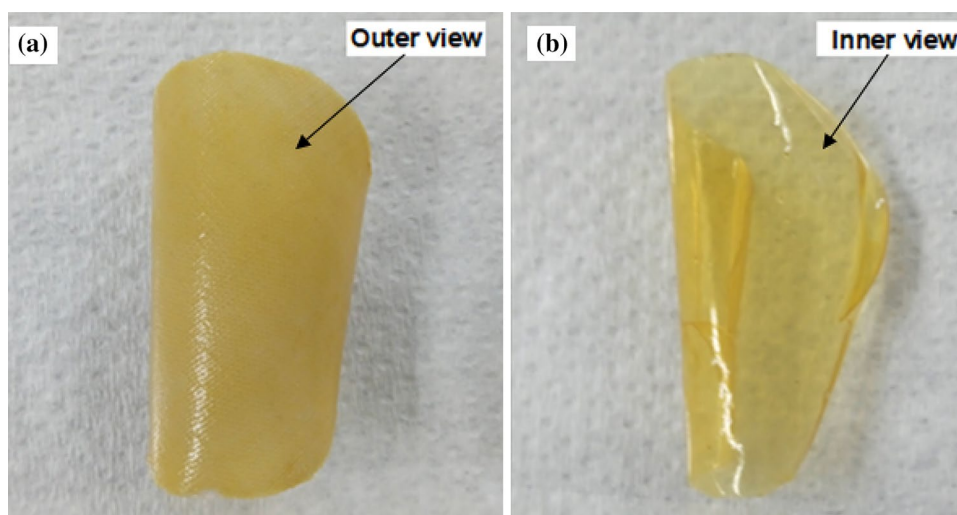
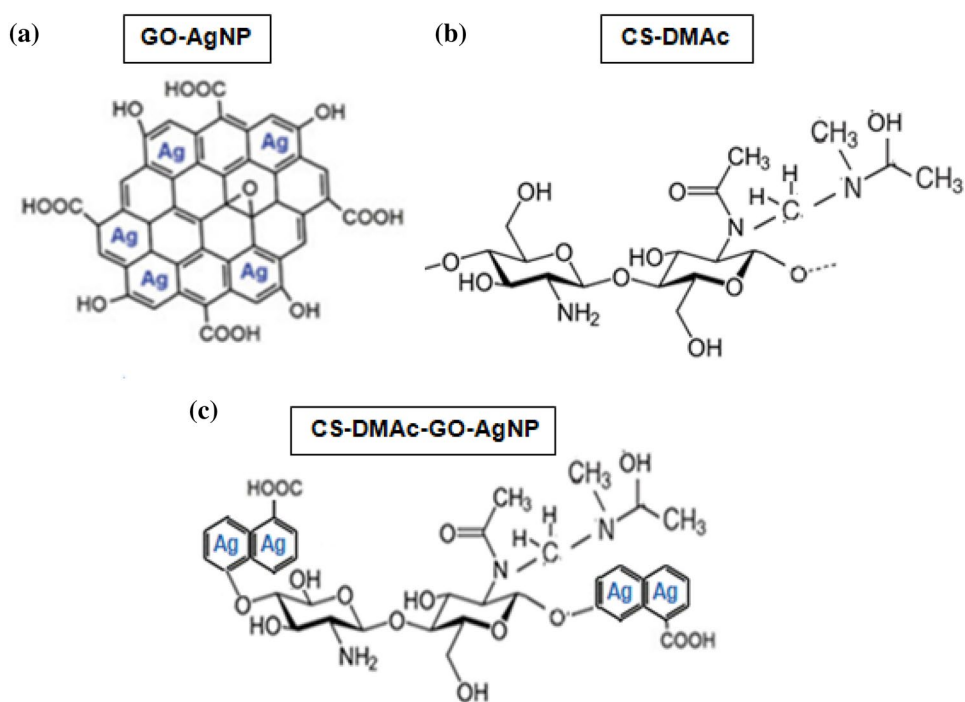


Fig. 3 Possible chemical interaction within modified CS composites



hydrogen bonds, which may have allowed for the entrapment of Ag nanoparticles on the membrane surface.

Characterization of Modified CS Nanocomposites

A Perkin Elmer (USA) spectrophotometer was used to record UV–visible absorption spectra. The thickness of the CS polymeric composites was measured using a Sylvac digital indicator. Owing to controlled layer by layer operations, the printed modified CS composite samples have average thickness of about 120 μm which could ensure structural integrity. The surface morphology of the composite samples were investigated using a Field Emission Scanning Electron Microscope (FESEM)-JSM-7900F model (Japan) which was coupled with an EDS Oxford Instrument for elemental surface analysis. X-ray diffraction (XRD) patterns of the produced membrane samples were acquired at room temperature by a Malvern Panalytical X'Pert –X-ray powder diffraction Philips (Malvern-UK) using Cu K-alpha radiation, running at 40 kV and 10 mA within the range of 0° to 90° (2 θ degree). FT-IR spectra (4000–500 cm^{-1}) were analyzed using Perkin Elmer Spectrum 100 FT-IR spectrometer measured at room temperature.

Microbiological Assessment of Modified CS Membranes

Microbiological analysis was conducted at Ambio Laboratories-VUT. The microbiological quantification of contaminated water samples for *E. coli*, Total Coliforms, and Fecal

Coliforms determination were prepared according to standard procedures [43]. The modified printed CS membranes were used for bacterial analysis by means of filtration kit equipped with a vacuum pump and operated at fixed pressure of 220 mmHg. Filtrates labeled B-9 to B-12 corresponding to various membrane samples were afterwards examined using Colilert reagent (IDX 3302-06/12) to determine the contamination level of the specified microorganisms in water samples. Total Coliforms and *E. coli* bacteria were evaluated using the Colilert technique, whereas Fecal Coliforms were detected using the MFC Agar plate counting method.

MFC Agar Plate Assay

The antibacterial performance of CS–GO–AgNP was evaluated to determine the inhibition capacity against Fecal coliforms using established procedure adapted by Gu et. al. [44], with some modification. Briefly, the bacteria were dispersed in sterile normal saline to produce a bacterial suspension containing 10^5 – 10^6 CFU/mL. 100 ml of the contaminated water samples (B-9 to B-12) were suctioned through the modified CS nanocomposite membrane samples placed on absorbable 0.45 μm grid membrane filter papers using a filtration apparatus. The membrane filter papers were thereafter placed on sterile Petri dishes impregnated with MFC agar that had been previously prepared. The agar plates were then incubated for 24 h at 37 degrees Celsius. After incubation period, the agar plates were removed from the incubator and number of bacterial colonies on the grid filter papers were counted with the aid of microscopic equipment and the

number of colony-forming units (CFU) per 100 ml sample was determined using the standard equation (Eq. 1). This experiment was conducted in triplicate with duplicates and the mean CFU levels were determined. The numerical values were translated to CFU per 100 ml.

$$\begin{aligned} \text{No. of CFU per 100 ml} \\ = (\text{No. of colonies on the membrane}) \\ / (\text{volume of sample filtered}) \times 100 \end{aligned} \quad (1)$$

Colilert-18 Assay

The use of Colilert-18 (QuantiTray/2000) approach for identifying *E. coli* and Total coliform bacterial cells has not been widely reported in any current studies. The Total coliforms and *E. coli* detection technique was performed according to the manufacturer's instructions. 100 ml of each filtrate sample (B-9 through B-12) was used for the Colilert experiment. After adding the reagent to the sample, it was put into Quanti-Tray/2000 (counts from 1 to 2419), sealed and incubated at 37 degrees Celsius for 24 h. The findings were then recorded in accordance with manufacturer instructions (IDEXX) and the Most Probable Number (MPN) was determined. Positive wells for Total coliform appeared yellowish than a comparator, while vivid blue fluorescent wells showed the presence of *E. coli* after the incubation period.

Design and Evaluation Process

The design and evaluation process of the modified Chitosan membranes in water filtration system is shown in Fig. 4 and depicted on the graphical abstract (Fig. 1). Step A is the modification process of Chitosan using AgNP/GO and DMAc. Stage B is the 3D printing of modified Chitosan. The third stage, (C) shows post treatment of the printed membranes. The final stage, (D) is the application of the composite membranes in inactivating bacterial strains in contaminated water via filtration process.

Table 1 shows the chemical components and their respective percentage weight compositions in the modified Chitosan ink formulation. Each sample's composition was ultrasonically treated for twenty minutes and then filtered to eliminate particles that had accumulated during the ink

Table 1 Percentage weight composition

Solution vol. (200 ml)	Chemical component	Sample B-9	Sample B-10	Sample B-11	Sample B-12
Solvent A (81 ml)	CS	85%	83%	81%	79%
	GO	0.3 ml	0.6 ml	0.9 ml	1.2 ml
	AgNP	0.3 ml	0.6 ml	0.9 ml	1.2 ml
	DMAc	15%	17%	19%	21%
Solvent B (119 ml)	Iso-alc	2%	2%	2%	2%
	H ₂ O	98%	98%	98%	98%

CS chitosan, GO graphene oxide, AgNP silver nanoparticles, Iso-alc Isopropyl alcohol, H₂O distilled water

formation process. Each sample's total solution volume was 200 ml. Chitosan (CS), graphene oxide (GO), silver nanoparticles (AgNP) and Dimethylacetamide make up Solvent A (81 ml). The 119 ml volume of solvent B includes isopropyl alcohol and distilled water. This percentage conforms to the 3D inkjet HP10 print-head specifications sheet. In terms of solvent A, the percentage mole fractions of CS/GO/AgNP and DMAc co-solvent were varied and compared. The samples are labeled B-9 through B-12 to show that they are within the printable range of an inkjet 3D printer, as determined by drop formation characteristics.

Results and Discussion

XRD Analysis of Modified CS Composites

Figure 5a displays the XRD patterns of samples B-9, B-10, B-11, and B-12, with the majority of broad peak diffractions occurring before the Bragg angle (2θ) 30.0°, which corresponds to 110 Ag crystal planes. The B-9 diffraction pattern revealed a small peak at 2 23.3°, which can be attributed to the addition of a minute quantity of AgNP to the composite sample. However, sample B-10 exhibited a single broad peak at 2 22.89°, which may be attributable to the increased intermolecular hydrogen bonds between CS chains and GO. The B-11 diffraction spectrum showed a broad peak at 2 21.57°, which could also be attributed to stronger hydrogen bond attraction of more AgNP with increase in the concentration of GO and DMAc in the CS polymer membrane sample. A sharp thin diffraction peak is observed at 2 29.30°



Fig. 4 Process flow diagram

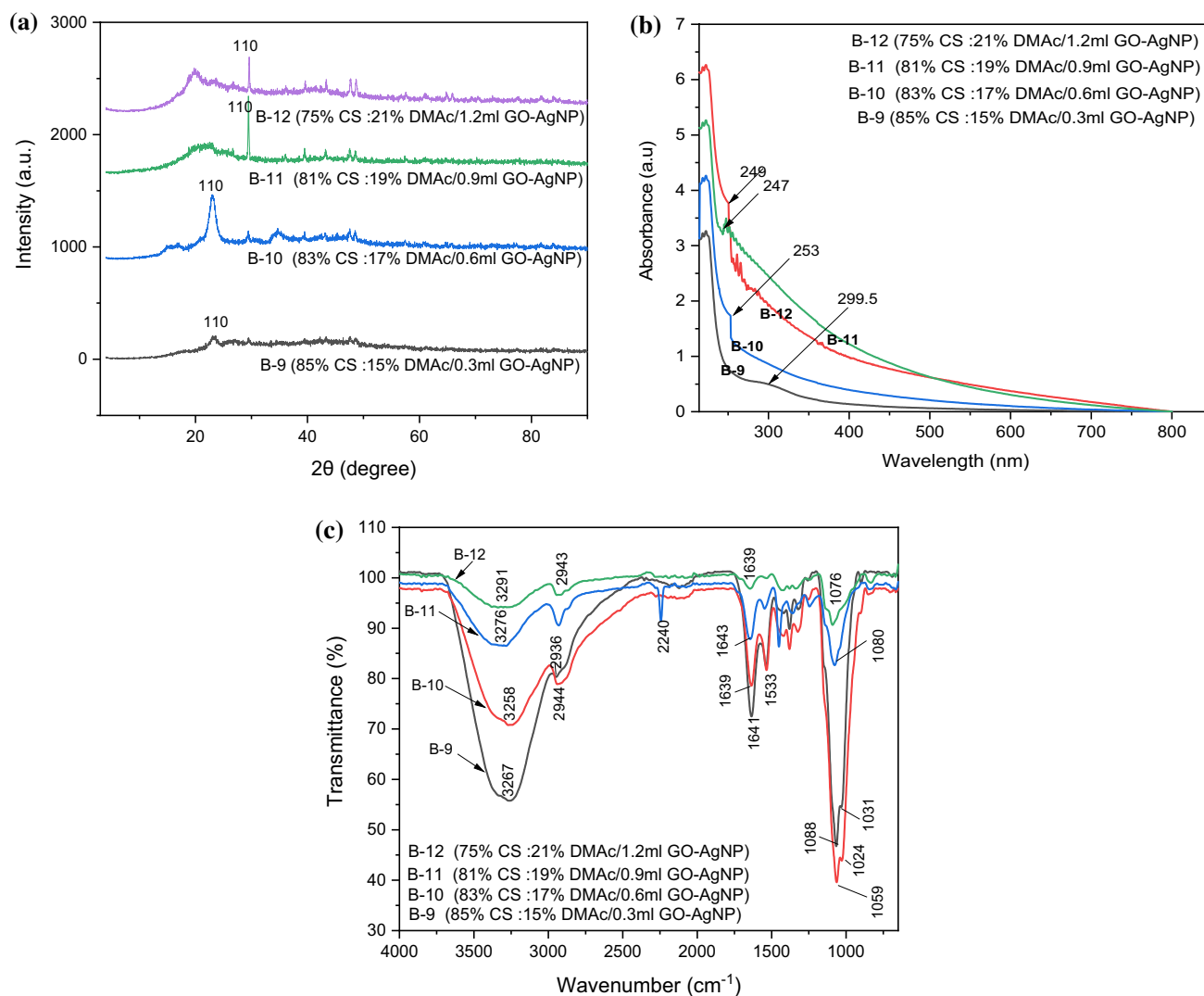


Fig. 5 **a** XRD patterns of the modified CS composite samples. **b** UV–VIS absorption spectra of the nanocomposites. **c** FT-IR analytical curves of CS composite samples

indicating strong attraction of AgNP to carbonyl groups of CS–GO–DMAc chemical bonding. Subsequently, there is a progressive reduction in d-spacing in sample B-11 which possibly implies loss of O–H functional groups around the borders of the membrane [45]. In addition, after the sorption of Ag^+ ions, sample B-12 displayed three characteristic sharp diffraction peaks, a large peak at 20.06° , a very sharp peak at 29.8° , and a minor peak at 48.7° , which correspond to the (110), (110), and (200) crystal planes of Ag, respectively [46]. This observation may suggest the transformation of adsorbed Ag^+ ions to AgO within the B-12 membrane network.

UV–VIS Analysis

The monitoring of the growth of silver-nanoparticles (AgNP) plasmon peaks in the modified CS fluid samples was observed using UV–VIS absorption spectra. Two characteristic peaks appeared in the 200–800 nm measurement range for all samples, as depicted in Fig. 5. The signal peak centered at 299.5 nm for B-9 might be ascribed π – π^* transitions of the oxime C=N bonds. The spectrum of B-10 displayed a characteristic peak at 253 nm towards the left side. Sample B-11's spectral peak at 247 nm could be attributed to π – n^* transitions of the C–C bonds in both samples, indicating the formation and successful deposition of AgNP onto GO within the modified CS matrix.

These peaks could arise because of surface plasmon resonance of Ag metal ions, which is one of the characteristics

of Ag metal, indicating that spherical shape AgNP was produced early on due to the existence of an amide bond from DMAc. The fluid sample of B-12 seemed to exhibit three typical peaks at 221 nm, 249 nm, and 261 nm, respectively. Figure 5b reveals that the peaks at 221 nm fall within the extinction spectrum of GO–AgNP to the left, ruling out nanocomposite aggregation during the formation of GO–CS–AgNP composite. The silver plasmon resonance peak increased gradually with increasing concentrations of GO–AgNP and DMAc in the ink formulation, which may be the result of an engraving process that causes a slight increase in the size of AgNP incorporated into the CS matrix. However, the concentration of AgNP fell further after roughly 350 nm due to an etching process [47].

FT-IR Analysis

As shown in Fig. 5, FT-IR was employed to detect the functional groups in the printed membrane samples. All of the samples (B-9 to B-12) exhibited broad and strong peaks of O–H bond between 3290 and 2936 cm^{-1} , which can be attributed to hydrogen bonds and overlapping bands of O–H in hydroxyl groups and N–H stretching in amino groups [48]. In contrast, there was a clear blue shift of –OH from 3258 to 3291 cm^{-1} (samples B-10 to B-12), indicating a stronger hydrogen bond as a result of an increase in the concentration of DMAc in the membrane ink formulation.

However, sample B-10 and B-11 showed isolated peaks at 1031 and 2240 cm^{-1} which possibly suggest traces of sulfur oxide (S=O) and C≡N nitrile bond [xxx]. In all samples, the peaks at 1639, 1643, 1639 and 1641 cm^{-1} correspond to the symmetric and asymmetric stretching of aliphatic –C=C– conjugated alkenes [45, 48]. The band between 1059 and 1088 cm^{-1} corresponds to the stretching of the C–O bond in primary alcohol, which may confirm the presence of a carbonyl group in CS–DMAc–GO/AgNP composites. Possible confirmation of the constituent functional groups in our modified Chitosan filtration membranes are the stretching vibration in primary amino groups (2936–2943 cm^{-1}) of CS, C–N stretching of amine in DMAc (1024–1031 cm^{-1}), N–H bending of hydrogen bond in CS–DMAc (2936–2943 cm^{-1}) and C–O stretching of residual acetyl groups in CS (1088–1076 cm^{-1}) respectively. Similarly, all samples exhibit asymmetric stretching of bridge C–O–C and C–O bonds in C–OH at 1088, 1059, 1080 and 1076 cm^{-1} .

The characteristic band for AgNP attachment would appear at 3258 to 3291 cm^{-1} (O–H stretching) and 1076–1088 cm^{-1} (C–O–C stretching) due to the tightly bound water oxygen-containing functional groups present in the modified Chitosan film.

SEM and EDS Analysis

SEM imaging was used to examine the surface morphologies of modified Chitosan membranes composite films. Figure 6a1–d1 depict, respectively, samples B-9, B-10, B-11 and B-12 with different surface structural arrangement. Figure 6a clearly shows more uniform layered structure, with greater homogeneity and thin film compared to other membrane samples which may suggest abundance of amine functional groups of CS on the surface. However, sample B-12 (Fig. 6d1) film has a distinctive sandwich structural layer that caused the surface to wrinkle as the concentrations of AgNP and GO increased. According to reports, this wrinkling characteristic retains high membrane surface area and prevents collapse of membrane structural network [49]. The influence of the hydroxyl and amino groups from CS–DMAc, which can engage and establish hydrogen bonds with the hydroxyl, carbonyl, and carboxyl moieties in the AgNP–CS–GO composite sheets, could be responsible for this result [50].

The structural morphology of each sample (B-9 to B-12) generally reveals varying levels of layer thickness, indicating that the film was not formed uniformly. This could suggest various stages of drop generation throughout the 3D printing process via layer by layer interfacial polymerization. According to literature report, 3D membranes have variable surface roughness and can improve transport performance with lower concentration polarization while reducing fouling, in contrast to traditional membranes, which generally have smooth surface morphologies [25, 51].

The development of amide connections between molecules of DMAc and CS could have allowed AgNP to scatter more equally in the modified chitosan matrix displayed as dotted white dots throughout CS surface layer from Fig. 6a–d. However, sample B-12 has a greater cloud of white packed structures than sample B-11 and other samples, which may indicate a higher surface concentration of AgNP. This may also suggest greater intermolecular force on the surface structure of the modified CS matrix which might have altered the original CS structure because of greater electrostatic interaction between the amide groups of DMAc–CS structure and the epoxy group of GO thereby preventing aggregation of AgNP in the modified CS composite membranes and improve AgNP contact with *E. Coli* and Coliform bacteria strains. The elemental composition of the modified 3D printed Chitosan nanocomposite samples were confirmed using EDS analysis as indicated in Fig. 6a2–d2. The EDS of B-9 (Fig. 6a2) spectrum 40 shows the following major elements detected on the surface of membrane sample, C (64%), N (19.1%), O (15%). The trace elements accessible are Ag (0.7%), S (0.2%), Si (0.1%) and Al (0.1%) respectively. The weight percentages of the two major elements C (59.6%) and O (39.0%) are

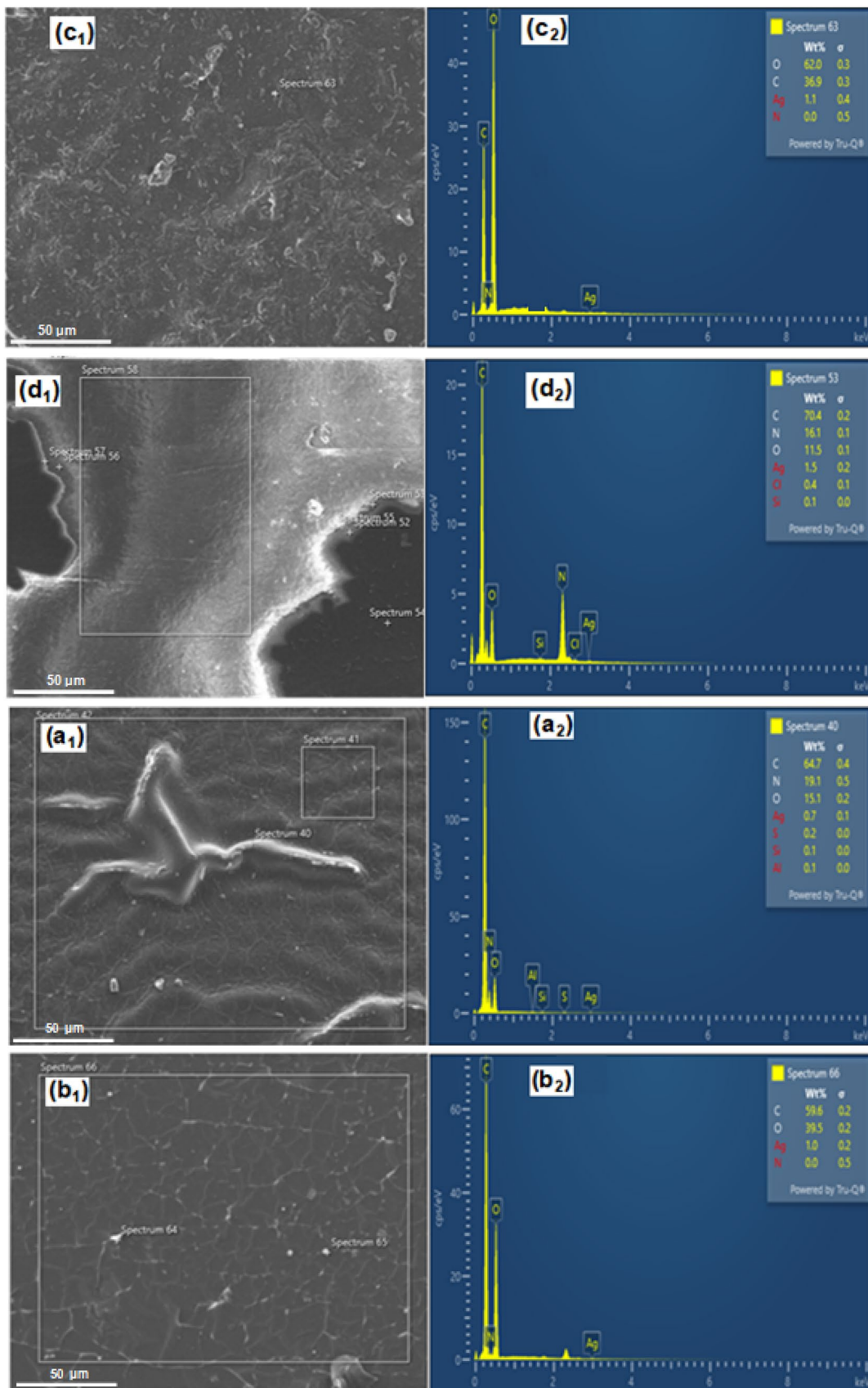


Fig. 6 SEM morphology and EDS elemental composition

displayed in Sample B-10. Ag (1%) was detected as minor element on the spectrum (Fig. 6b2). As shown in spectrum 63, the atomic percentages obtained from EDS analysis of sample B-11 indicate that Oxygen comprises 62.0%, Carbon contains 36.9% and Silver has 1.1%. Sample B-12 shows an improved adsorption of AgNP on the surface of the modified Chitosan membrane as indicated in spectrum 53 (Fig. 6d2). The weight percentage of each element on the composite sample includes 70.4% C, 16.1% N, 11.5% O and 1.5% Ag. Other trace elements detected are Cl (0.4%) and S (0.1%) respectively.

The gradual increase in the percentage of Ag peaks by EDS spectra from sample B-9 to B-12 is the confirmation of the chelating ability of the prepared CS–GO–AgNP composites and also one of the effects of increasing the concentrations of AgNP–GO in the ink formulation. Furthermore rise in the quantity of DMAc in the CS matrix could have led to the augmentation of the carbon content from sample B-10 to B-12. The existence of trace elements of Si, S, Cl and Al peaks could be attributed to the presence of residues or impurities from compounds such as H_2SO_4 , HCl and SiO_2 which were utilized for ink preparation or in contact with the modified CS composite during membrane post treatment process.

Fecal Coliforms Analysis

Blue colonies of varying shades were detected on all samples as illustrated in Fig. 7a–f. These are regarded to be colonies of Fecal Coliforms which depict various coliforms concentration on each membrane sample. After 24 h of incubation, the negative control—an MFC membrane filter containing 20 ml of sterile water—showed no evidence of a blue colony. However, the positive control in Fig. 7b shows that entire surface area of membrane was completely surrounded by large blue colonies of Fecal Coliforms after incubation period.

According to CFU/100 calculation, more than 10, 000 fecal coliforms were found in 100 ml of the infested water. Other samples showed reduced number of Fecal colonies in comparison with the positive control. Samples B-9 (Fig. 7c) has 700 CFU/100 ml, sample B-10 has 300 CFU/100 ml (Fig. 7d), sample B-11 contained 200 CFU/100 ml (Fig. 7e), while sample B-12 indicated 120 CFU/100 ml respectively as shown in Fig. 7f. This trend may reflect improved anti-bacterial activity of the modified Chitosan in restricting the number of Fecal Coliforms in the filtered water samples. It may also imply that increasing the concentrations of GO–AgNP and subsequently decreasing the mole fraction of CS in the membrane ink formulation could increase the reduction of Fecal Coliforms in water. In addition, DMAc co-solvent may also contribute to the enhanced antibacterial

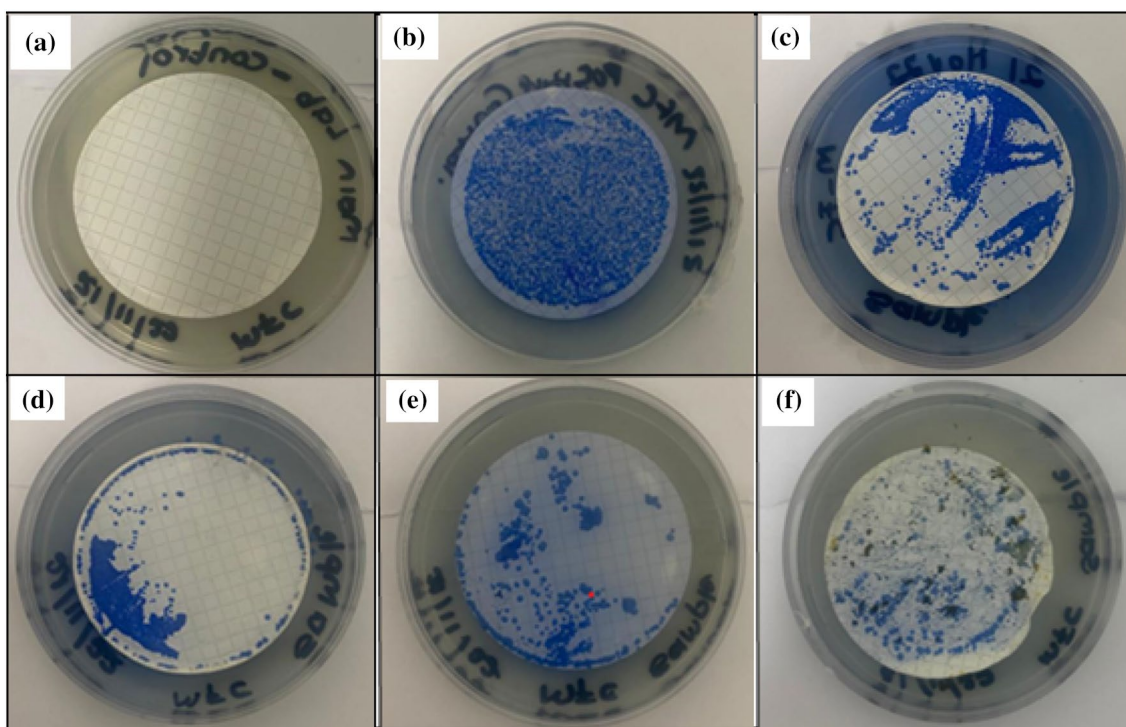


Fig. 7 Fecal coliforms characterization

activity of the membrane samples by enhancing the formation of hydrogen bonds.

The analytical results further revealed that samples B-11 and B-12 indicated lesser growth of the Fical Coliforms compared to B-10 and B-9. This may indicate a larger concentration of AgNP on the nanocomposites, which upon contact deactivated and perhaps killed the bacterial strains. This may also suggest that the epoxy-amino groups with a stronger hydrogen bond in the CS membrane network may have electrostatically interacted with the negatively charged cellular membranes of Fecal bacteria strains, resulting in a greater penetration through the bacteria wall and a consequent inhibition of their growth [52].

Total Coliforms and *E. coli* Analysis

Figure 8a–f shows different concentrations of Total coliforms from the samples. Positive control (Fig. 8b) contains more than 2420 MPN Total Coliforms in 100 ml of water according to MPN chart. The sterile control Fig. 8a did not indicate any Yellow well and subsequently has 0

MPN/100 ml. The filtrate samples of the modified CS composites showed gradual reduction of Total coliforms concentration in 100 ml of water from Fig. 8c–f. This could suggest that CS/GO/AgNP composite membrane has an improved antibacterial effect in suppressing Coliform bacteria in water. Antibacterial activity improved with increase in the concentration of GO–AgNP and decrease in the amount of CS in the formulation. The co-solvent (DMAc) could have adequate plasticizing effect on the membranes which strengthened the cohesive intermolecular bond that prevented seeping of the bacterial strains from the surface of CS membrane network into the filtrates.

E. coli detection was visible in all the incubated IDEXX Quanti-Tray samples except for sterile water sample Fig. 8a. The absence of *E. coli* microorganisms in the sample could have caused the Wells not to illuminate blue fluorescent when passed through the UV light. This consequently suggests that the sterile water was void of *E. coli*, hence negative control with 0 MPN/100 ml of water. Figure 8b shows complete blue fluorescent Wells indicating possible positive

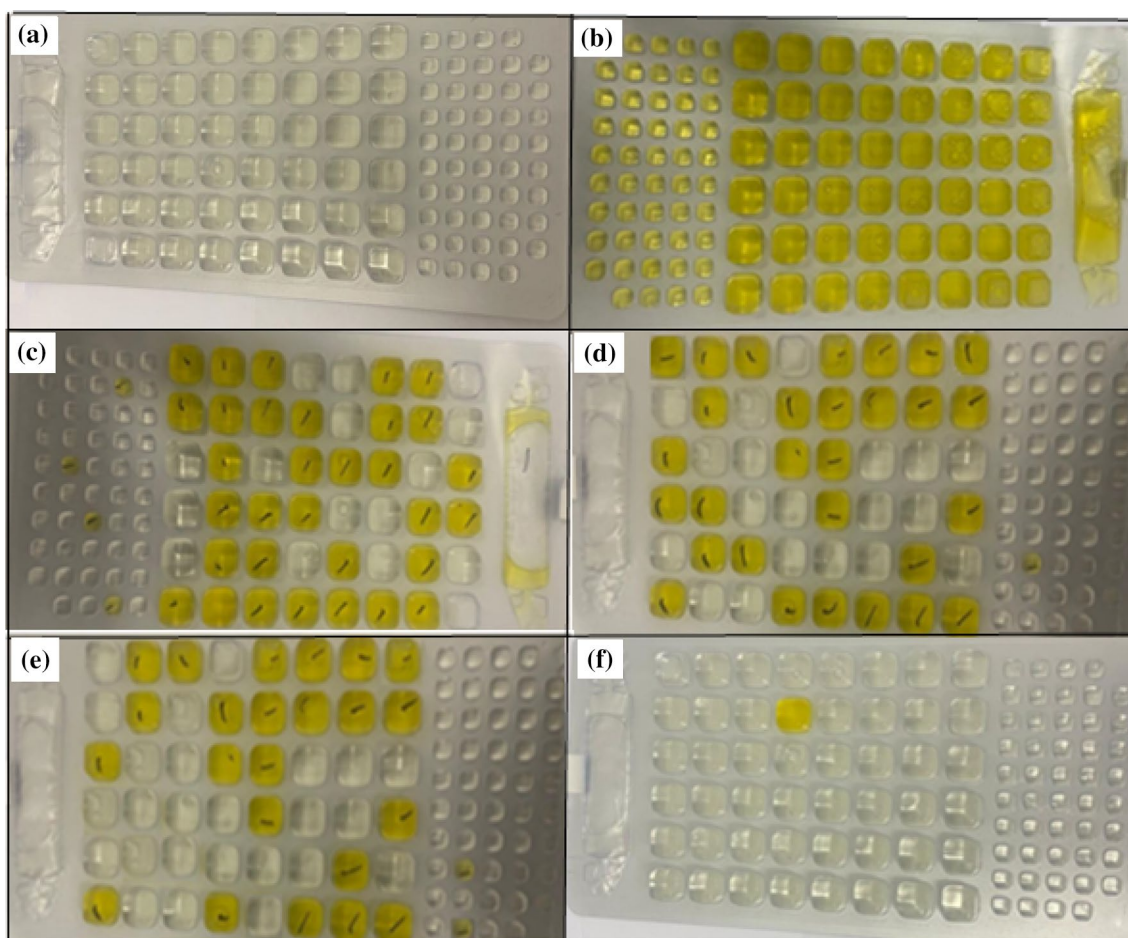


Fig. 8 Development of yellow color Wells in Colilert-18 Quanti-Tray/2000

Table 2 Quantification of bacterial analysis

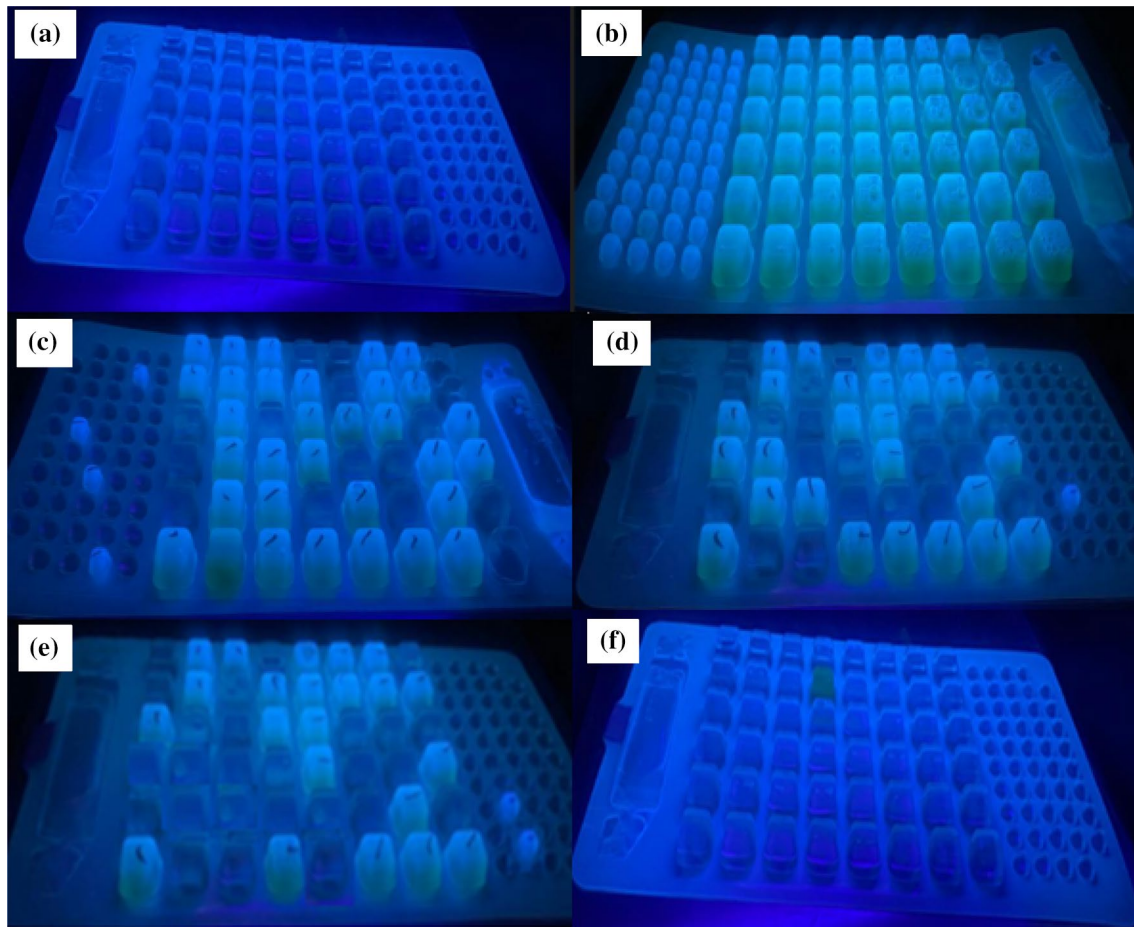
Sample	B-9	B-10	B-11	B-12	Saline control	Positive control
<i>E. coli</i> conc. (MPN/100 ml)	52.9 ± 0.6	38.9 ± 0.3	30.9 ± 0.5	0.0 ± 0.04	0.0 ± 0.02	> 2420 ± 0.2
Total Coliform (MPN/100 ml)	55.6 ± 0.5	43.2 ± 0.4	32.7 ± 0.2	1 ± 0.03	0.0 ± 0.01	> 2420 ± 0.4
Fecal Coliform (CFU/100 ml)	700 ± 1.2	300 ± 0.9	200 ± 0.5	120 ± 0.3	0 ± 0.03	> 10,000 ± 0.6

for *E. coli* detection with more than 2420 MPN/100 ml found in water sample using the IDEXX MPN table.

The observation from remaining samples Fig. 8c–f shows reduction in the concentrations of *E. coli* dictation in water samples. The number of positive wells with blue fluorescent light counted decreased from B-9 to B-12 indicating that *E. coli* concentration declined as the amount of GO–AgNP increased as shown in Table 2. Sample B-12 with the highest concentration of GO–AgNP and DMAc prevented *E. coli* completely in water (Fig. 8f). Hence this could suggest that *E. coli* microorganisms can be effectively controlled in using CS/GO/AgNP membrane filters. Furthermore the surface area of the membranes could have reduced with the addition

of more DMAc in the ink formulation which was added to improve stability and mechanical strength of the membrane samples (Fig. 9).

Table 2 shows the quantification of bacterial cells detected by the microbiological assessment of the modified CS membranes. The results showed decline in *E. coli*, Fecal Coliforms and Total Coliforms detected by the nanocomposite samples. This trend could suggest that the membrane samples increased their inhibition capabilities with increase in the GO–AgNP–DMAc concentration. The activities of microorganisms reduced from sample B-9 to B-12 with *E. coli* being suppressed most in the analysis. According to previous report, increase in CS layer may serve as a barrier

**Fig. 9** Development of blue-white fluorescence Wells under UV light in Colilert-18 Quanti-Tray/2000

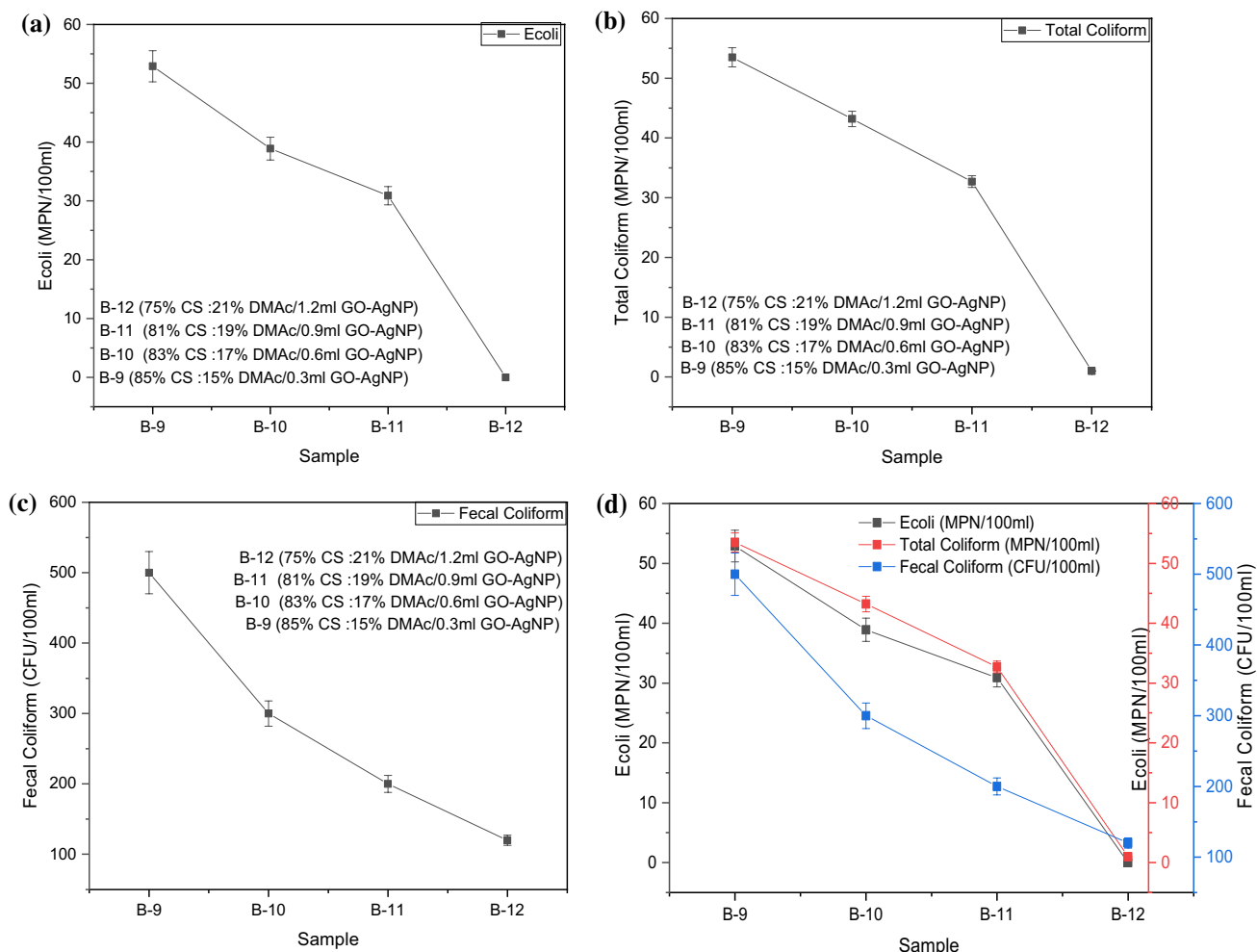


Fig. 10 Antibacterial analysis of modified CS composites

against chitosan-microbial interactions [53, 54]. This consequently might have contributed to decreased antimicrobial activity in samples B-9 and B-10 with greater amount of CS than in B-11 and B-12 composites.

Figure 10a shows the relationship between average *E. coli* concentration in 100 ml of water and the effectiveness of using the 3D modified CS membranes for controlling bacteria in water through filtration. The efficiency of the modified membranes could depend mainly in the ink formulation process. B-9 (79% CS, 21% DMAc/ 0.3 ml GO–AgNP) has the highest *E. coli* concentration of 52.9 MPN about per 100 ml of water. This indicates that mole percentage of *E. coli* microorganisms in the filtrate sample was about 2.19% of the total *E. coli* originally present in 100 ml of the contaminated water. Sample B-9 membrane could have killed or prevented 97.8% of the initial *E. coli* in water. Sample B-12 (85% CS, 15% DMAc/ 1.2 ml GO–AgNP) exhibited the least amount of zero contaminant level of *E. coli* concentration.

This suggests tremendous improvement in suppressing *E. coli* bacteria as indicated in Fig. 10a. Antibacterial properties of CS/GO/AgNP membranes might have reduced the level of water contamination by *E. coli* the activity through filtration.

Similarly, Total Coliforms in the water samples reduced with enhancement in the concentration of GO–AgNP in the modified membrane filters. Figure 10b shows a gradual linear decline in the Total Coliforms from B-9 to B-11 before a sharp decrease is observed in B-12. This could possibly suggest a wider spread of AgNP across the surface area of the membrane (sample B-12). The graph of Fecal Coliforms against samples B-9 to B-12 is shown in Fig. 10c. A steep gradient is observed between B-9 to B-10 though with higher number of Fecal Coliform observation than in B-11 and B-12. This may be attributed to adequate decline in the bacterial activity as more contact was made with CS–GO–AgNP nanocomposites. Samples B-11 and B-12 indicated lesser activity of Fecal bacteria with total

number of 200 CFU/100 ml and 120 CFU/100 ml respectively. Figure 10d shows the combination of the three bacterial strains examined in this study. Sample B-9 indicates lowest antibacterial activity of the CS nanocomposites for Fecal Coliforms, Total Coliforms and *E. coli* strains, followed by sample B-10 and B-11. Sample B-12 shows maximum impact of the CS composites against the three bacterial strains.

Antimicrobial Activities and Mechanism of Modified CS

Comparative antibacterial study of the modified CS membrane components was determined to establish the antimicrobial mechanism using the Colilert-18 IDEXX assay [55, 56]. Briefly, the test procedure consists of the following steps: introducing 100 mL of filtrate sample and the dehydrated Colilert -18 medium into a sterile plastic bottle and pouring the mixture into a tray (Quanti-Tray /2000); sealing the tray and incubating it at 35 °C for 24 h; counting the positive wells (yellow wells that become fluorescent under 365 nm UV light indicate the presence of *E. coli*, finally, a matrix correlates the numbers of positive wells (small and big) with the most probable number (MPN) of *E. coli* present in the analyzed sample. The amount of CS (100%wt), GO (0.5 wt%) and AgNP (0.5 wt%) remained unchanged throughout the comparative study. Similarly the concentration of microorganisms used for the experiment was not altered. To ensure the reproducibility of the results, each experiment was conducted in triplicate.

The average concentration values of *E. coli* and Total coliform detected from the filtrate samples of CS, CS–GO, CS–AgNP and CS–GO–AgNP membranes respectively after 24 h of incubation are shown in Table 3.

CS composite displayed the highest concentration of bacterial cells (89.6 ± 0.32 MPN/100 ml) detected after the incubation period when compared to other membrane components which obviously suggests that CS exhibited weak inhibition of the bacterial activities. This result is in conformity with other reported observations which pointed out the weak antimicrobial effect of CS membranes [57]. The addition of GO and AgNP unto CS displayed improved performance of antimicrobial performance of CS matrix as evident in the reduced concentration values of *E. coli* and Total Coliforms.

However CS–AgNP nanocomposite shows more significant antibacterial activity than CS–GO. This could suggest that AgNP at constant amount of CS would improve the antibacterial activities than GO since Chitosan membrane network enhances the immobilization of Ag ions and consequently improved contact killing of the microorganisms as supported by earlier studies [50, 58]. Moreover, it was also previously reported that the interaction between CS and AgNP facilitates the release of silver ions from AgNP which contributes to the improved antimicrobial effect of modified Chitosan composite [59].

The combined effects of CS–GO–AgNP on *E. coli* and Total Coliform revealed tremendous reduction of the bacterial activities after incubation period as depicted in Fig. 10. The average concentration of *E. coli* reduced to 34.3 ± 0.33 MPN/100 ml, while that of Total coliform dropped to 48.6 ± 0.41 MPN/100 ml, indicating improved inhibition capacity of CS–GO AgNP composite membrane.

The statistical data in Fig. 11 further illustrates speedy decline in *E. coli* concentration than Total coliform concentration. This could be attributed to greater attraction of the gram negative bacterial cells towards the modified CS membrane network with increased concentration of Ag-GO thereby causing rapid bacterial cell inactivation. However the combination of CS–GO–AgNP composite shows tremendous antibacterial activity against *E. coli* and Total Coliform strains by reducing their concentration from 40.8 to 34.3

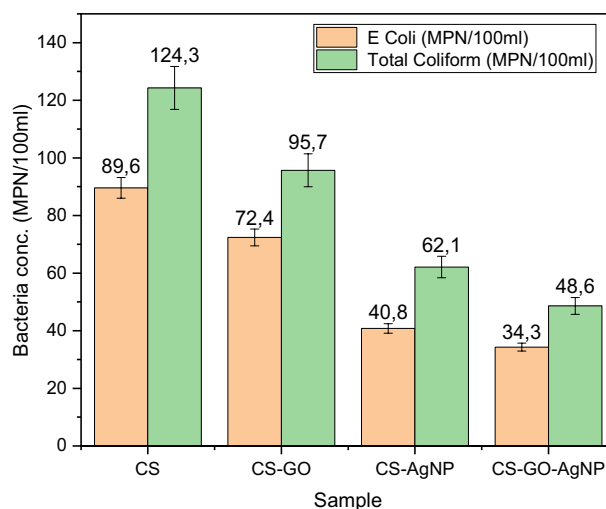


Fig. 11 Antibacterial statistical data of modified CS components

Table 3 Antibacterial analysis of modified CS components

Sample	CS	CS–GO	CS–AgNP	CS–GO–AgNP	Saline control	Positive control
<i>E. coli</i> conc. (MPN/100 ml)	89.6 ± 0.32	72.4 ± 0.81	40.8 ± 0.75	34.3 ± 0.33	0.0 ± 0.03	$> 2420 \pm 0.5$
Total Coliform (MPN/100 ml)	124.3 ± 0.48	95.7 ± 0.43	62.1 ± 0.29	48.6 ± 0.41	0.0 ± 0.01	$> 2420 \pm 0.7$

MPN/100 ml (*E. coli*) and 62.1 to 48.6 MPN/100 ml (Total Coliforms) respectively. Consequently the comparative results revealed that CS–GO–AgNP composite membrane exhibited the highest synergetic effects than individual an component which is also in conformity with literature report [60]. Therefore we utilized the combination of all the components in the 3D printing of our filtration membranes.

The possible antibacterial mechanisms of CS, CS–GO, CS–AgNP and CS–GO–AgNP nanocomposite against *E. coli* and Total Coliforms bacterial strains based on the quantitative result of the Colilert-18 IDEXX experiment is shown on Fig. 12. The mechanism was suggested in four different stages to illustrate the antimicrobial activities for each membrane component. In the first phase, each active bacterial cell present in the contaminated water came in contact with CS composite. Chitosan was able to disrupt the barrier properties of few outer cells of gram-negative bacteria. Previous literature predicted that the electrostatic interaction between positively charged R-N(CH₃)₃⁺ sites of CS and negatively charged microbial cell membranes was responsible for cell inactivation and therefore assumed as the main antimicrobial mechanism [61]. However due to weaker antimicrobial strength of CS it could only destroy few cell-membranes of microorganisms attached to its surface as shown in Fig. 11 (stage 1). This is because CS is very porous

with low stability and poor mechanical strength [62]. In the second phase, inactivation of bacterial cells increased further on contact with CS–GO surface. The increase in deactivation of bacteria strain between CS–GO could be due to hydrogen-bonding between the oxygen-containing groups of GO and amine groups of CS that resulted nucleophilic substitution reactions between the amine and oxygen containing groups of GO which have capacity to induce oxidative pressure that ruptures cell membrane [63, 64].

Phase 3 mechanism (CS–AgNP) indicates increased number of inactivated microorganisms with the inclusion of AgNP, which led to greater impact on the bacterial cells causing speedy penetration and destruction microbial cell walls [65]. The combined effects of CS–AgNP–GO composite (phase 4) showed further improvement of antibacterial impact against the microorganisms possibly because of increased hydrogen bonding within the CS–GO–AgNP structure leading to the entrapment of the negatively charged cell walls of *E. coli* and Coliforms bacteria unto the surface of more positively charged modified CS. Furthermore, CS–AgNP–GO composite membranes provides improved structural network for the attachment sites for AgNP into abundance reactive oxygen species from CS–GO interaction allowing Ag nanoparticles direct contact with bacterial cell

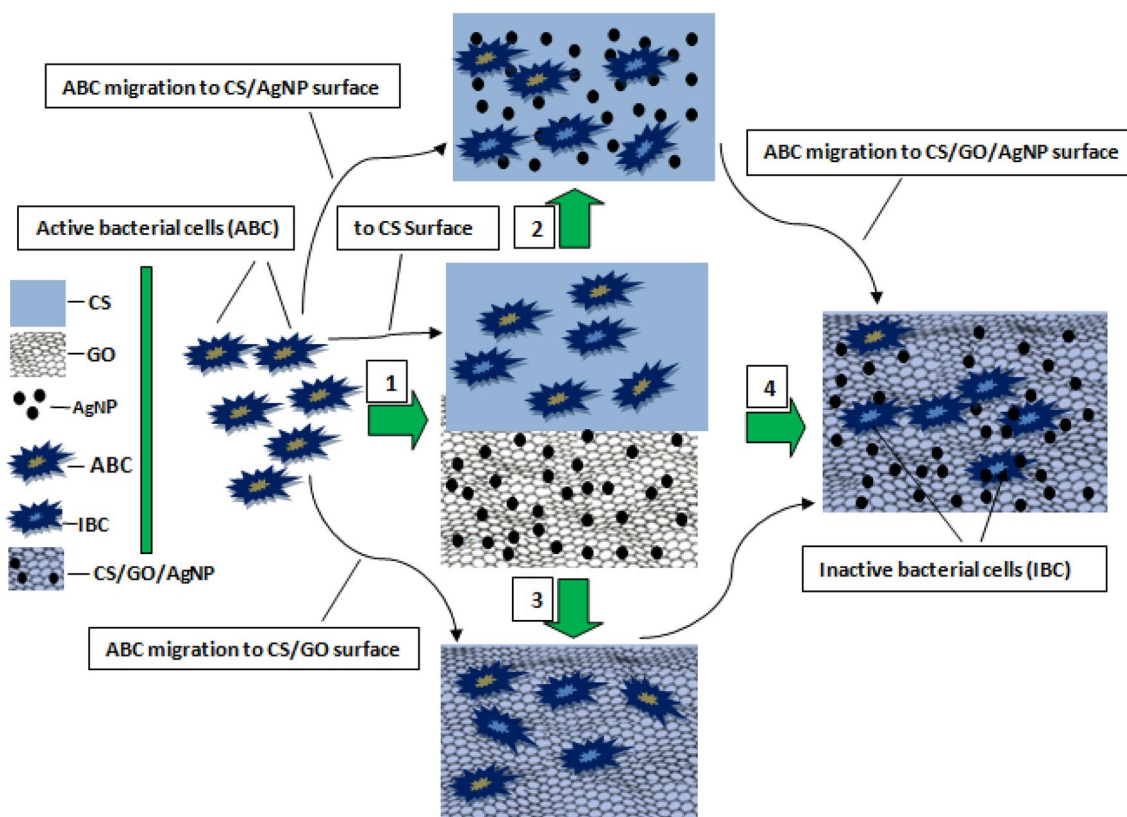


Fig. 12 Mechanism of antimicrobial activities

walls thereby preventing membrane fouling as supported by previous studies [14, 66].

Confirmation Tests

Membrane Tube Fermentation process was used for verification tests. The rear of the Quanti-Tray packets was cleaned with 70% alcohol and the contents extracted using a sterile syringe. Fecal Coliforms were confirmed by scraping off the colonies on top of the agar with a sterile loop for the MF method. *E. coli* was confirmed by gas and indole production in lactose tryptose lauryl sulphate broth, while Total Coliforms were confirmed by gas production in lactose broth. The initial leaching test of silver-nanoparticles from the CS–GO–AgNP composite films during filtration of contaminated water samples was observed by UV–VIS spectra analytical technique. Each filtrate sample was examined for traces of Ag nanoparticles.

Our results revealed no significant leaching of AgNP to the filtrates after filtration as evidenced by observing no peak in the range of 240–340 nm as shown in Fig. 13 which was earlier identified as the main zones of AgNP resonating peaks in the modified CS composites (Fig. 5b). Additionally, strong hydrogen bond resulting from the chemical interaction between the epoxy groups of GO and the amide groups of CS–DMAc may have immobilized the Ag nanoparticles

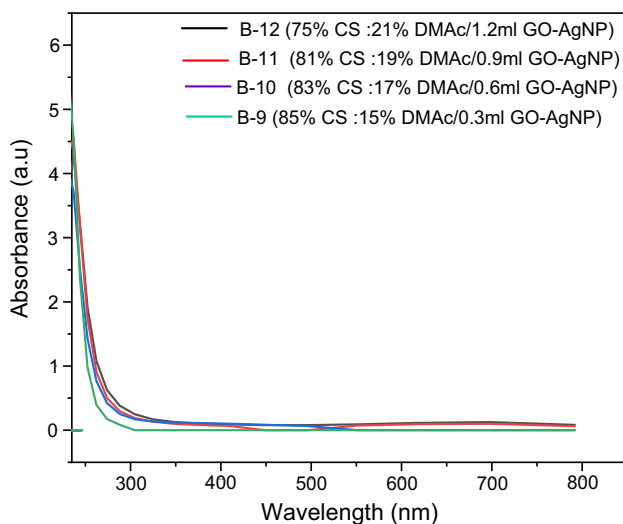


Fig. 13 Qualitative analytical Ag leaching test

Table 4 Quantification of Ag concentration

Sample	B-9	B-10	B-11	B-12
Ag in CS matrix (mL/200 mL)	0.3 ± 0.02	0.6 ± 0.01	0.9 ± 0.03	9.2 ± 0.02
Ag conc. in CS matrix (mg/L)	1.5 ± 0.05	3.0 ± 0.02	4.5 ± 0.01	6.0 ± 0.04
Ag conc. in effluent (mg/L)	0.035 ± 0.03	0.032 ± 0.001	0.026 ± 0.002	0.021 ± 0.001

in the composite, resulting in negligible leaching of AgNP from the composite films [67].

The stability of immobilized silver nanoparticles on the surface of modified CS membrane was further quantified using a dynamic leaching technique adopted by Zhu et al. [58]. Briefly, samples B9 to B12 were introduced sequentially into this system, and the leaching process continued until no more silver leaching was observed in the effluent solution. The system was fed with DI water at a flow rate of 2.5 mL/min. Every 30 min for the first two hours, effluent samples were taken. ICP-MS was used to assess the silver amounts in effluent samples. Table 4 compares the leaching test outcomes and the starting concentration of Ag nanoparticles in modified CS composite samples. There is a considerable decrease in the quantity of Ag that leaked into the effluent, with B-12 exhibiting the greatest drop at 0.021 mg/L (0.35%) than other membrane samples.

Conclusions

The effects of 3D printed modified chitosan on preventing identified bacterial cells were carefully revealed in this study. The gradual increase in the concentration of GO–AgNP improved antibacterial activities of the nanocomposite membranes by inhibiting the growth and multiplication of Total Coliforms, Fecal Coliforms and *E. coli* bacterial strains in water, thus demonstrating improved antibacterial activity that can possibly prevent biofouling. The enhanced antimicrobial activity of the modified CS from B-9 to B-12 resulted from a combination of different mechanisms such as toxicity exhibited by the individual component in CS–AgNP–GO nanoparticles, such as the lipid of CS, cell permeability mechanisms influenced by the presence of GO sheets. Therefore, the immobilization of Ag nanoparticles within CS–GO–AgNP nanocomposite was attributed to the stability of the modified CS matrix which also helped to prevent bacterial formation and growth during filtration process.

Furthermore, increase in concentration of DMAc improved the chemical structure and the physical properties of Chitosan by escalating the number of participating hydroxyl and amino chains responsible for hydrogen bonding within CS–GO–AgNP composite. This suggests that the printed membrane samples possessed greater contact with bacteria due to increase in the DMAc concentration which is attributed to the improved tensile strength of CS composites. Also DMAc could have adequate plasticizing effect on the membranes which might strengthen the cohesive intermolecular

bond by preventing the microorganisms from seeping through the surface of CS membrane network into the filtrates. The surface morphological assessment showed greater dispersion of AgNP across the modified CS layers while the elemental analysis revealed gradual increase in the percentage of Ag peaks within the CS composites with enhance in the concentration of GO–AgNP. Therefore, our 3D printed membranes can effectively be applied to control Total Coliforms, Fecal Coliforms and *E. coli* bacteria in surface water.

Acknowledgements The authors gratefully acknowledge the technical assistance and financial support by the Faculty of Engineering and Technology, Vaal University of Technology Gauteng.

Author Contributions ACO conducted the experiments, prepared the figures/ tables and wrote the main manuscript, while Prof POO supervised the entire practical work and reviewed the manuscript.

Funding Open access funding provided by Vaal University of Technology.

Declarations

Competing Interests The authors declare no competing interests.

Open Access This article is licensed under a Creative Commons Attribution 4.0 International License, which permits use, sharing, adaptation, distribution and reproduction in any medium or format, as long as you give appropriate credit to the original author(s) and the source, provide a link to the Creative Commons licence, and indicate if changes were made. The images or other third party material in this article are included in the article's Creative Commons licence, unless indicated otherwise in a credit line to the material. If material is not included in the article's Creative Commons licence and your intended use is not permitted by statutory regulation or exceeds the permitted use, you will need to obtain permission directly from the copyright holder. To view a copy of this licence, visit <http://creativecommons.org/licenses/by/4.0/>.

References

- World Health Organization (2003) Guidelines for safe recreational water environments. Coastal and fresh waters, vol 1. World Health Organization, Geneva
- ISO 9308-2 (2012) Water Quality- Enumeration of *Escherichia coli* and Coliform Bacteria: Part 2: Most Probable Number Method. International Organization for Standardization (ISO), Geneva, Switzerland
- De Faria AF, Martinez DS, Meira SMD, Moraes AC, Brandelli A, Souza AGF, Alves OL (2014) Anti-adhesion and antibacterial activity of silver nanoparticles supported on graphene oxide sheets. *Colloids Surf B* 113(2014):115–124
- Qayyum S, Khan AU (2016) Nanoparticles vs. biofilms: a battle against another paradigm of antibiotic resistance. *Med Chem Comm* 7(2016):1479–1498
- Monte-Serrano M, Fernandez-Saiz P, Ortí-Lucas R, Hernando B (2015) Effective antimicrobial coatings containing silver-based nanoclays and zinc pyrithione. *J Microb Biochem Technol*. <https://doi.org/10.4172/1948-5948.1000245>
- Pal P, Pal A, Nakashima K, Yadav BK (2021) Applications of chitosan in environmental remediation: a review. *Chemosphere* 266:128934
- Huang M, Tu H, Chen J, Liu R, Liang Z, Jiang L et al (2018) Chitosan-rectorite nanospheres embedded aminated polyacrylonitrile nanofibers via shoulderto-shoulder electrospinning and electrospaying for enhanced heavy metal removal. *Appl Surf Sci* 437(2018):294–303
- Spoială A, Ilie C, Ficai D, Ficai A, Andronescu E (2021) Chitosan-based nanocomposite polymeric membranes for water purification—a review. *Materials* 2021(14):2091. <https://doi.org/10.3390/ma1409209>
- Qian X, Li N, Wang Q, Ji S (2018) Chitosan/graphene oxide mixed matrix membrane with enhanced water permeability for high-salinity water desalination by pervaporation. *Desalination* 438(2018):83–96. <https://doi.org/10.1016/j.desal.2018.03.031>
- Marta B, Potara M, Iliut M, Jakab E, Radu T, Imre-Lucaci F, Katona G, Popescu O, Astilean S (2015) Designing chitosan–silver nanoparticles–graphene oxide nanohybrids with enhanced antibacterial activity against *Staphylococcus aureus*. *Colloids Surf A* 487:113–120
- Hui K, Dinh D, Tsang C, Cho Y, Zhou W, Hong X, Chun HH (2014) Green synthesis of dimension-controlled silver nanoparticle-graphene oxide with in situ ultrasonication. *Acta Mater* 64:326–332
- Wang LS, Wang CY, Yang CH, Hsieh CL, Chen SY, Shen CY, Wang JJ, Huang KS (2015) Synthesis and anti-fungal effect of silver nanoparticles–chitosan composite particles. *Int J Nanomed* 10:2685
- Song B, Zhang C, Zeng G, Gong J, Chang Y, Jiang Y (2016) Antibacterial properties and mechanism of graphene oxide–silver nanocomposites as bactericidal agents for water disinfection. *Arch Biochem Biophys* 604:1–10. <https://doi.org/10.1016/j.abb.2016.04.0180003-9861>
- Khawaja H, Zahir E, Asghar MA, Asghar MA (2018) Graphene oxide, chitosan and silver nanocomposite as a highly effective antibacterial agent against pathogenic strains. *Colloids Surf A*. <https://doi.org/10.1016/j.colsurfa.2018.06.052>
- Goda ES, Elella MHA, Sohail M, Singu BS, Pandit BE, Shafey AM, Aboraia AM et al (2021) N-methylene phosphonic acid chitosan/graphene sheets decorated with silver nanoparticles as green antimicrobial agents. *Int J Biol Macromol* 182(2021):680–688
- Pounraj S, Prathap S, Paul S (2018) Chitosan and graphene oxide hybrid nanocomposite film doped with silver nanoparticles efficiently prevents biofouling. *Appl Surf Sci* 452(2018):487–497. <https://doi.org/10.1016/j.apsusc.2018.05.009>
- Tan X, Rodrigue DA (2019) Review on porous polymeric membrane preparation. Part I: Production techniques with polysulfone and poly (Vinylidene Fluoride). *Polymers* 11:1160
- Yanar N, Kallem P, Son M, Park H, Kang S, Choi HA (2020) New era of water treatment technologies: 3D printing for membranes. *J Ind Eng Chem* 91:1–14
- Sang JL, Dong NH, Min H, Mi HD, Lee SuA, Park J-H, Kwon IK (2017) Most simple preparation of an inkjet printing of silver nanoparticles on fibrous membrane for water purification: technological and commercial application. *J Ind Eng Chem* 46(2017):273–278
- Zhou L, Fu J, He YA (2020) Review of 3D printing technologies for soft polymer materials. *Adv Funct Mater* 30:2000187
- Herzberger J, Serrine JM, Williams CB, Long TE (2019) Polymer design for 3D printing elastomers: recent advances in structure, properties, and printing. *Progress Polym Sci* 97:101144
- Low Z-X, Chua YT, Ray BM, Mattia D, Metcalf IS, Patterson DA (2017) Perspective on 3D printing of separation membranes and comparison to related unconventional fabrication techniques. *J Membr Sci* 523(2017):596–613
- Ji D, Xiao C, Chen K, Zhou F, Gao Y, Zhang T, Ling H (2021) Solvent-free green fabrication of PVDF hollow fiber MF

- membranes with controlled pore structure via melt-spinning and stretching. *J Membr Sci* 621:118953
24. Badalov S, Oren Y, Arnusch CJ (2015) Ink-jet printing assisted fabrication of patterned thin film composite membranes. *J Membr Sci* 493(2015):508–514
 25. Seo J, Kushner DI, Hickner MA (2016) 3D printing of micropatterned anion exchange membranes. *ACS Appl Mater Interfaces* 8:16656–16663
 26. Yusoff NHM, Chong CH, Wan YK, Cheah KH, Wong VL (2022) Optimization strategies and emerging application of functionalized 3D-printed materials in water treatment: a review. *J Environ Chem Eng* 10:108581
 27. Bergamonti L, Bergonzi C, Graiff C, Lottici PP, Bettini R, Elviri L (2019) 3D printed chitosan scaffolds: a new TiO₂ support for the photocatalytic degradation of amoxicillin in water. *Water Res*. <https://doi.org/10.1016/j.watres.2019.07.008>
 28. Zhou G, Wang KP, Liu HW, Wang L, Xiao XF, Dou DD, Fan YB (2018) Three-dimensional polylactic acid @ graphene oxide/chitosan sponge bionic filter: Highly efficient adsorption of crystal violet dye. *Int J Biol Macromol* 113(2018):792–803
 29. Decker C (2002) Kinetic study and new applications of UV radiation curing. *Macromol Rapid Commun* 23(18):1067–1093
 30. Sangermano M, Razza N, Crivello JV (2014) Cationic UV-curing: technology and applications. *Macromol Mater Eng* 299(7):775–793
 31. Hancock A, Lin L (2004) Challenges of UV curable ink-jet printing inks—a formulators perspective. *Pigm Resin Technol* 33(5):280–286
 32. Wahab MY, Muchtar S, Arahman N, Mulyati S, Riza M (2019) The effects of solvent type on the performance of flat sheet polyethersulfone international conference on science and innovated engineering (I-COSINE). *IOP Conf Ser* 536:012119. <https://doi.org/10.1088/1757-899X/536/1/012119>
 33. Zhu C, Zhou Y, Zhao H, Farajtabar A (2020) Thiamethoxam in aqueous co-solvent mixtures of 1,4-dioxane, N, N-dimethylacetamide, dimethyl sulfoxide and acetonitrile: solubility solute-solvent and solvent-solvent interactions, and preferential solvation analysis. *J Chem Thermodyn* 150:106229
 34. Ramanujam BTS, Parag BT, Adhyapak V, Radhakrishnan S, Marimuthu R (2020) Effect of casting solvent on the structure development, electrical, thermal behavior of polyvinylidene fluoride (PVDF)–carbon nanofiber (CNF) conducting binary and hybrid nanocomposites. *Polym Bull* 78:1735–1751. <https://doi.org/10.1007/s00289-020-03176-6>
 35. Karimia A, Khataeaa A, Vatanpour V, Safarpoure M (2020) The effect of different solvents on the morphology and performance of the ZIF-8 modified PVDF ultrafiltration membranes. *Separ Purif Technol* 253:117548
 36. Yang H, Acharya S, Abidi N (2018) Cellulose porosity improves its dissolution by facilitating solvent diffusion. *Int J Biol Macromol* 123:1289–2129
 37. Ogazi AC, Osifo PO (2023) Effects of dimethylacetamide on chitosan/AgNP/GO fluid properties for 3D printing of water filtration membranes. *Polym Adv Technol* 2023:1–11. <https://doi.org/10.1002/pat.5964>
 38. Hummers WS, Offeman RE (1958) Preparation of graphene oxide. *J Am Chem Soc* 80:1339
 39. Faria A, Lui C, Xie M, Perreault F, Nghiem L, Ma J, Elimelech M (2017) Thin-film composite forward osmosis membranes functionalized with graphene oxide–silver nanocomposites for biofouling control. *J Membr Sci* 525:146–156
 40. Karimia A, Khataeaa A, Vatanpour V, Safarpour M (2020) The effect of different solvents on the morphology and performance of the ZIF-8 modified PVDF ultrafiltration membrane. *Sep Purif Technol* 253:117548
 41. Ramanujam BTS, Parag V, Adhyapak S, Radhakrishnan S, Marimuthu R (2021) Effect of casting solvent on the structure development, electrical, thermal behavior of polyvinylidene fluoride (PVDF)–carbon nanofiber (CNF) conducting binary and hybrid nanocomposites. *Polym Bull* 2021(78):1735–1751. <https://doi.org/10.1007/s00289-020-03176-6>
 42. Eugster R, Rosatzin T, Rusterholz B, Aebbersold B, Pedrazza U, Denise R, Schmid A, Ursula E, Spichiger U, Simon W (1994) Plasticizers for liquid polymeric. *Anal Chim Acta* 289:1–13
 43. U.S. Environmental Protection Agency (2009) Method, 1603. *Escherichia coli (E. coli)* in water by membrane filtration using modified membrane-thermotolerant *Escherichia coli* Agar (modified m TEC). EPA-821-R-09–007. Office of Water, U.S. Environmental Protection Agency, Washington, D.C
 44. Bin Gu, Jiang Q, Luo B, Liu C, Ren J, Wang X, Wang X (2021) A sandwich-like chitosan-based antibacterial nanocomposite film with reduced graphene oxide immobilized silver nanoparticles. *Carbohydr Polym* 260:117835
 45. Xue J, Wang S, Han X, Wang Y, Hua X, Li J (2018) Chitosan-functionalized graphene oxide for enhanced permeability and antifouling of ultrafiltration membranes. *Chem Eng Technol* 41:270–277
 46. Mohan YM, Vimala K, Thomas V, Varaprasad K, Sreedhar B, Bajpai SK, Raju KM (2010) Controlling of silver nanoparticles structure by hydrogel networks. *J Colloid Interface Sci* 342:73–82
 47. Marta B, Potara M, Iliut M, Jakob E, Radu T, Imre-Lucaci F, Katona G, Popescu O, Astilean S (2015) Designing chitosan–silver nanoparticles–graphene oxide nanohybrids with enhanced antibacterial activity against *Staphylococcus aureus*. *Colloids Surf A* 487(2015):113–120
 48. Pawlak A, Mucha M (2003) Thermogravimetric and FTIR studies of chitosan blends. *Thermochim Acta* 396(2003):153–166
 49. Wu H, Wang J, Kang X, Wang C, Wang D, Liu J, Aksay IA, Lin Y (2009) Glucose biosensor based on immobilization of glucose in platinum nanoparticles/graphene/chitosan nanocomposite film. *Talanta* 80:403–406
 50. Rajoka MS, Zhao L, Mehwish HM, Wu Y, Mahmood S (2019) Chitosan and its derivatives: synthesis, biotechnological applications, and future challenges. *Appl Microbiol Biotechnol* 103(2019):1557–1571. <https://doi.org/10.1007/s00253-018-9550-z>
 51. Chowdhury MR, Steffes J, Huey BD, McCutcheon JR (2018) 3D printed polyamide membranes for desalination. *Science* 361:682–686
 52. Zhang X, Li Y, Guo M, Jin TZ, Arabi SA, He Q, Ismail BB, Hu Y, Liu D (2021) (2021) Antimicrobial and UV blocking properties of composite chitosan films with curcumin grafted cellulose nanofiber. *Food Hydrocoll* 112:106337
 53. Zheng L-Y, Zhu J-F (2003) Study on antimicrobial activity of chitosan with different molecular weights. *Carbohydr Polym* 54:527–630
 54. Eaton P, Fernandes JC, Pereira E, Pintado ME, Malcata FX (2008) Atomic force microscopy study of the antibacterial effects of chitosans on *Escherichia coli* and *Staphylococcus aureus*. *Ultramicroscopy* 108:1128–1134
 55. Tiwari A, Niemelä SI, Vepsäläinen A, Rapala J, Kalso S, Pitkänen T (2016) Comparison of Colilert–18 with miniaturized most probable number method for monitoring of *Escherichia coli* in bathing water. *J Water Health* 14:121–131
 56. Vergine P, Salerno C, Barca E, Berardi G, Pollice A (2016) (2016) Identification of the faecal indicator *Escherichia coli* in wastewater through the β-D-glucuronidase activity: comparison between two enumeration methods, membrane filtration with TBX agar, and Colilert® -18. *J Water Health* 15:209

57. Spoială A, Ilie C-I, Dolete G, Croitoru A-M, Surdu V-A, Trus R-D, Motelica L et al (2022) Preparation and characterization of Chitosan/TiO₂ composite membranes as adsorbent materials for water purification. *Membranes* 12:804. <https://doi.org/10.3390/membranes12080804>
58. Zhu X, Bai R, Wee K, Liu C, Tang S (2010) Membrane surfaces immobilized with ionic or reduced silver and their anti-biofouling performances. *J Membr Sci* 363(2010):278–286
59. Biao L, Tan S, Wang Y, Guo X, Fu Y, Xu F, Zu Y, Liu Z (2017) Synthesis, characterization and antibacterial study on the chitosan-functionalized Ag nanoparticles. *Mater Sci Eng C* 1(76):73–80. <https://doi.org/10.1016/j.msec.2017.02.154>
60. Pounraj S, Somu P, Paul S (2018) Chitosan and graphene oxide hybrid nanocomposite film doped with silver nanoparticles efficiently prevents biofouling. *Appl Surf Sci* 452(2018):487–497
61. Rabea EI, Badawy ME, Stevens CV, Smagghe G, Steurbaut W (2003) Chitosan as antimicrobial agent: applications and mode of action. *Biomacromol* 4:1457–1465
62. Vakili M, Rafatullah M, Salamatinia B, Abdullah AZ, Ibrahim MH, Tan KB, Gholami Z, Amouzgar P (2014) Application of chitosan and its derivatives as adsorbents for dye removal from water and wastewater: a review. *Carbohydr Polym* 113:115–130
63. Qiu J, Geng H, Wang D, Qian S, Zhu H, Qiao Y, Qian W, Liu X (2017) Layer-number dependent antibacterial and osteogenic behaviors of graphene oxide electrophoretic deposited on titanium. *ACS Appl Mater Interfaces* 9:12253–12263
64. Wei Y, Zhang X, Gao X, Ma Z, Wang X (2018) Multilayered graphene oxide membranes for water treatment: a review. *Carbon* 139(2018):964–981. <https://doi.org/10.1016/j.carbon.2018.07.040>
65. Ramalingam B, Parandhaman T, Das SK (2016) Antibacterial effects of biosynthesized silver nanoparticles on surface ultrastructure and nanomechanical properties of gram-negative bacteria viz. *Escherichia coli* and *Pseudomonas aeruginosa*. *ACS Appl Mater Interfaces* 8(7):4963
66. Bin Gu, Jiang Q, Luo B, Liu C, Ren J, Wang X, Wang X (2021) A sandwich-like chitosan-based antibacterial nanocomposite film with reduced graphene oxide immobilized silver nanoparticles. *Carbohydr Polym* 260(2021):117835
67. Kim JS, Kuk E, Yu KN, Kim JH, Park SJ, Lee HJ, Kim SHYK, Park YH, Hwang CY et al (2007) Antimicrobial effects of silver nanoparticles. *Nanomedicine* 3(2007):95–101

Publisher's Note Springer Nature remains neutral with regard to jurisdictional claims in published maps and institutional affiliations.